THE ASTROPHYSICAL JOURNAL, 491:L55–L58, 1997 December 10

YOHKOH SXT OBSERVATIONS OF X-RAY "DIMMING" ASSOCIATED WITH A HALO CORONAL MASS EJECTION

ALPHONSE C. STERLING[1,2]
Computational Physics, Inc., 2750 Prosperity Avenue, Suite 600, Fairfax, VA 22031; asterling@solar.stanford.edu
AND
HUGH S. HUDSON[2]
Solar Physics Research Corp., 4720 Calle Desecada, Tucson, Arizona 85718; hhudson@solar.stanford.edu
Received 1997 May 7; accepted 1997 October 10; published 1997 November 6

ABSTRACT

A sudden depletion or intensity "dimming" of the X-ray corona sometimes accompanies a solar eruptive flare or coronal mass ejection (CME). We have identified a dimming that occurred just prior to a "halo" CME, observed on 1997 April 7 using the Soft X-ray Telescope (SXT) on *Yohkoh*. Halo CMEs are prime candidates for "space weather" effects. The dimming occurred in compact regions near a flare of 14 UT on April 7, over a projected area of about 10^{20} cm^{-2}, and indicate that a mass of a few times 10^{14} g was ejected. This is a lower limit imposed by the obscuration of the dimming volume by the brightness of the accompanying flare and other factors. Most of the mass deficit comes from two regions close to the ends of a preflare S-shaped active-region structure, and the resulting dimmings in these regions persisted for more than three days following the flare. A cusp-shaped loop—not apparent prior to the flare—dominates the emission in the flare decay phase, and has a mass comparable to that lost in the dimming regions. Our findings are consistent with the source of the CME being a flux rope that erupted, leaving behind the dimming regions. The cusp-shaped loop probably represents magnetic fields reconfigured or reconnected by the eruption. We do not see an X-ray analog of the wavelike disturbance evident in *SOHO* EUV images.

Subject headings: Sun: corona — Sun: flares — Sun: particle emission — Sun: X-rays, gamma rays

1. INTRODUCTION

Coronal mass ejections (CMEs) originate in the solar corona, and the *Yohkoh* soft X-ray observations have shown that at least a portion of the ejected mass can sometimes be detected in X-rays during its outward motion (Hudson, Acton, & Freeland 1996). More commonly, however, the best X-ray signature of the launching of a CME may be an intensity "dimming" that is analogous to the coronal depletions originally detected in white light by Hansen et al. (1974; see Hudson & Webb 1997). (For reviews of CMEs, see, e.g., Kahler 1992; Hundhausen 1993; Gosling 1996; Low 1997. Rust & Hildner 1976 discuss dimming in *Skylab* X-ray data.)

Here we describe *Yohkoh* observations of a dimming event that coincided with a "halo" CME. Such a CME appears to a white-light coronagraph (ideally) as a diffuse cloud that symmetrically surrounds the solar occulting disk. The natural interpretation of such an event, borne out by observations of disturbances in the solar wind near the Earth, is that a halo CME represents an ejection directed along the Sun-Earth axis (Howard et al. 1982). Such CMEs have been difficult to detect with a coronagraph because of the scattering geometry (although they can currently be observed by the LASCO coronagraphs on *SOHO*), which favors CMEs at the limb. These Earthward-moving events are the geophysically most important, in the context of space weather–related phenomena, and indeed, the event that we describe here did produce auroral activity. Such events are capable of major disturbances of the Earth's magnetosphere, causing power disruptions (e.g., McAllister et al. 1996) and other effects. As far as we are aware, this event is the first in the literature in which X-ray imaging showed direct evidence for coronal mass loss associated with a halo CME.

2. OBSERVATIONS

We use observations from the *Yohkoh* soft X-ray telescope (SXT; Tsuneta et al. 1991), which produces about 50 complete, full-Sun images per day. In spite of gaps caused by orbital motion and other effects, this often provides a sufficient frequency of observation to detect the X-ray signatures related to a CME, such as X-ray dimmings (see Hudson & Webb 1997 for details).

This study centers on observations of the soft X-ray (~1–2 keV) corona associated with a flare peaking at 14:00 UT on 1997 April 7. This was a *GOES* class C6.8 flare, as shown in Figure 1, which occurred in NOAA active region 8027. The next available images from the LASCO coronagraph on *SOHO* showed a "halo" CME at 14:27 UT (C. St. Cyr 1997, private communication). The flare was also spatially and temporally associated with a large-scale coronal wave phenomenon observed by the EUV telescope EIT on *SOHO*. In addition, there were interplanetary observations, including type II and type III coronal and interplanetary radio bursts and particle events observed by the *Wind* satellite, originating near 14:00 UT (D. Berdichevsky et al., private communication). An extrapolation of the height-time curve indicates that the southwest component of the LASCO halo CME crossed 1 $R_\odot$ (along the Earth-Sun line of sight) location at about 14:10 UT (R. A. Howard 1997, private communication). These observations provide strong evidence that the halo CME was associated with the 14 UT flare and the soft X-ray features and dimmings that we discuss here. As we will show below, our dimming analysis is also consistent with CME mass being ejected from the region near the flare.

Yohkoh missed the impulsive phase of the flare because of spacecraft night, and so there was no opportunity to observe

[1] Also E. O. Hulbert Center for Space Research, Naval Research Laboratory, Washington, DC.
[2] Current address: Institute for Space and Astronautical Science, Yoshinodai 3-1-1, Sagamihara, Kanagawa 229, Japan.

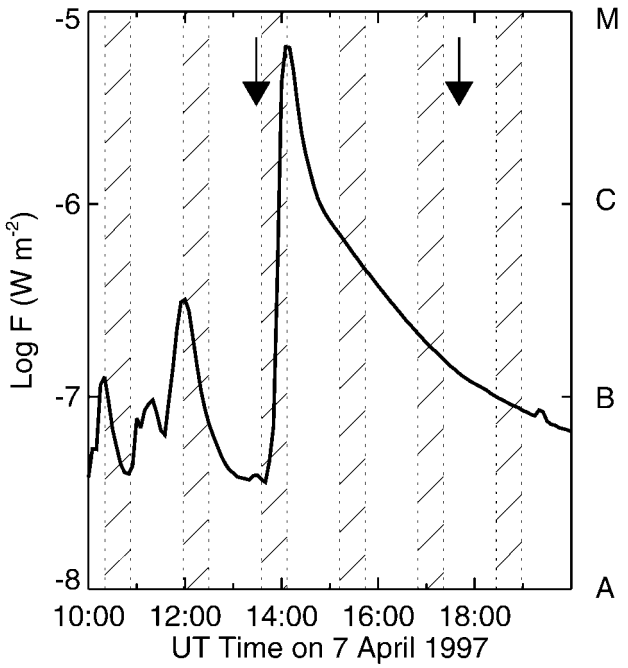

FIG. 1.—Soft X-ray flux from the 1–8 Å channel of *GOES 9* during the launch of the CME. *Arrows:* times of *Yohkoh* SXT images shown in Fig. 2; *hatched regions:* intervals of *Yohkoh* orbit night.

mass that may have been ejected at that time directly (see Shibata et al. 1995). Difference images from before and after the event, however, may show the effect of coronal dimming. In an event on the solar disk (as opposed to a limb event, for which the background solar brightness is less), such a detection is problematic because of the proximity of the flare brightening. Flaring causes two serious systematic effects in the SXT data with regard to CME dimming observations: the flare can trigger "flare mode," in which long-duration, wide-field exposures are not taken by SXT; and the flare brightness itself can cause degradation of the fainter parts of the images (viz., the periphery of the active region or the adjacent quiet corona) via scattered X-rays. An event reported by Hiei, Hundhausen, & Sime (1993) provided a clear example of coronal dimming in a large-scale streamer event off the disk (Hudson 1996). In that case there was a relatively faint and diffuse brightening, and the scattered–X-ray background was low.

3. DIMMING ANALYSIS

Figures 2*a* and 2*b* (Plate L2) show SXT AlMg filter images from before the flare (Fig. 1, *first arrow*) and late in the decay phase of the flare (Fig. 1, *second arrow*), respectively, and Figure 2*c* shows the difference image formed by subtracting the image in Figure 2*a* from that in Figure 2*b*. In the preflare image, the flaring region is dominated by a bright S-shaped structure, but there are several fainter features. Comparison with magnetograms from Kitt Peak shown in Figure 3 (Plate L3) indicates that the northwestern part of this structure is anchored in a negative magnetic polarity, the bright body of the S sits atop a positive polarity region, and the southeastern portion of the S curls back to point at this positive polarity region. During the flare decay in Figure 2*b*, the predominant feature is a cusp-shaped structure that approximately straddles the magnetic inversion line, rooted in the opposite polarities. In Figure 2*b* the contour indicates the 40% level intensity contour of Figure 2*a*. We do not see this preflare S-shaped structure in the postflare image, although we would expect to be able to see it if it still existed, since its intensity was only about a factor of 5 fainter than that of the cusp at the time of Figure 2*b*. The footpoints of the preflare and postflare structures appear to be connected to the same locations, although this cannot be inferred very precisely from these data. Therefore, the preflare S-shaped structure may have physically evolved into the loop arcade and cusp by the time of the postflare image of Figure 2*b*.

In the difference image of Figure 2*c* the cusp is prominent. On either side of the cusp are darker regions that constitute the dimming, that is, regions in which preflare material has been ejected and is now absent. Figure 2*d* is identical to Figure 2*c*, except in that it is overlaid with contours marking some of the regions where the dimming is substantial, labeled R1, R2, and R3. We also mark two "control" regions for comparison, R4 and R5, where there is no apparent dimming; both of these regions have the same shape as R1 and are located symmetrically relative to the flare, thus providing a similar level of scattered X-rays. One more region, R6, outlines the entire postflare loop structure (which we take to be the brightest 75% of the Fig. 2*b* image). We determined an emission measure, $\mathrm{EM} \approx N_e^2 V$, where N_e is the electron number density and V is the emitting volume, from the flux of the SXT images for each of these regions and used this to estimate the amount of contained mass. Spectral data are as described in Tsuneta et al. (1991), and we assume a hydrogen plasma with equal proton and electron number densities. Table 1 gives the resulting emission measures, along with derived densities and mass values, where we have assumed $V = A^{3/2}$ for each region, and A is the area defined in Figure 2*d*. SXT's data cadence with different filters was too low to allow direct determination of temperatures prior to the flare, and during the flare decay, the flux in the dimmed regions is too low to admit reliable temperature estimates without involved considerations of scattering in the images. Results for R1–R5 in Table 1 assume a temperature of 3 MK, which is typical of high-altitude structures in weak active regions (e.g., Sterling, Hudson, & Watanabe 1997). We give the preflare mass values in the fifth column of Table 1 and the difference in the calculated masses (preflare minus postflare) in the sixth column.

Summing the preflare masses for regions R1–R3 results in a total mass of about 3.2×10^{14} g, which is similar to that found in other dimming studies (Hudson & Webb 1997; Hudson et al. 1996; those works reported preflare masses only). Summing the amount of mass lost in those regions (i.e., the preflare masses minus the postflare masses) yields 1.5×10^{14} g, under the above assumptions. If we alter our assumed temperatures to be 2.0 or 4.0 MK, we find instead total preflare mass values of 6.9 or 2.4×10^{14} g, respectively, and in total, mass-loss values of 3.0 or 1.1×10^{14} g, respectively, for the dimming regions. These values should be regarded as lower limits, since (i) any dimming of the corona directly above the flare would be obscured by the flare itself; (ii) we have made no corrections for scattered light in the later images, when the flare structure is brighter; (iii) there could have been continued outflow in the dimmed regions; and (iv) the SXT broadband response has a bias toward higher temperatures (temperatures derived for similar active regions from X-ray spectroscopic data, however, are close to those found by SXT; Brosius et al. 1997; Sterling 1997). Our results for R4 and R5 indicate an uncertainty in the mass estimates resulting from scattering of X-rays to be of order 1×10^{13} g. Estimates of typical CME masses from co-

TABLE 1
DERIVED PARAMETERS FOR REGIONS OF FIGURES 2*a* AND 2*d*[a]

Region	V ($\times 10^{29}$ cm^3)	Emission Measure ($\times 10^{45}$ cm^{-3})	N_e ($\times 10^{8}$ cm^{-3})	Mass[b] ($\times 10^{14}$ g)	ΔMass[c] ($\times 10^{14}$ g)
R1	0.52	79.0	12.3	1.1	0.4
R2	1.19	40.5	5.8	1.2	0.5
R3	2.01	14.2	2.7	0.9	0.6
Total	3.72	133.7	...	3.2	1.5
R4	0.52	3.7	0.7	0.06	−0.06
R5	0.52	2.5	0.9	0.08	−0.03
R6	2.58	1556.0	24.5	10.6	...
R_s	2.64	327.1	11.1	4.9	...

[a] Emission measure, N_e, and masses. Calculated assuming 3 MK temperature for R1–R5 and R_s and 3.4 MK for R6.
[b] Preflare (13:29 UT) masses for R1–R5, postflare (17:41 UT) for R6. R_s is for the preflare S-shaped structure (13:29 UT).
[c] Preflare (13:29 UT) minus postflare (17:41 UT) mass difference.

ronagraph observations range from 10^{15} to 10^{16} g (e.g., Kahler 1992).

We can use the same technique to examine the amount of mass in the entire postflare structure, specifically in region R6 in Figure 2*d*. This region is bright enough to allow a temperature determination using the SXT filter-ratio technique (see Tsuneta et al. 1991), which yields a temperature of 3.4 MK. Using the observed intensity and the same $A^{3/2}$ assumption for volume as above, we find a mass of about 1.1×10^{15} g and $N_e \approx 2.4 \times 10^9$ cm^{-3}, as shown in Table 1. From the bright S-shaped preflare feature (75% contour of Fig. 2*a*), we estimate a mass of 10.8, 4.9, and 3.8×10^{14} g for temperatures of 2.0, 3.0, and 4.0 MK, respectively. Thus, the mass in the preflare structure is comparable to the mass in the cusp-shaped flare decay-phase structure. Other properties are listed for this structure as the R_s entry of Table 1.

We have also investigated the time series of the partial-frame SXT images in flare mode (14:08–14:18 UT) and of the full-disk difference images for wavelike structures emanating from the flaring region. A radially propagating structure, perhaps an EUV counterpart to a "Moreton wave" (originally defined in terms of chromospheric observations; Athay & Moreton 1961), has been reported in *SOHO* EIT 195 Å Fe XII images (J. Gurman & B. Thompson 1997, private communication; the *SOHO* data will be reported elsewhere). We were unable to find evidence for the wave in SXT data in the Al or AlMg filters, covering approximately 3–20 Å, which may indicate that it was not hot enough to be seen in soft X-rays, even though it is clearly visible in the EUV images. SXT has a broadband response with temperature (Tsuneta et al. 1991) and tends to see higher temperatures than the Fe XII images, which have a narrower peak near 1.6 MK (Delaboudinière et al. 1995). SXT does see temperatures down to at least 2 MK in diffuse coronal structures, however, and so some other factor may be responsible for the nonsighting in SXT. For example, only two useful full-disk SXT images were obtained during the EIT wave observation period, at 14:19 and 14:38 UT, meaning that SXT may have missed the wave because of poor data coverage. Also, SXT images typically have a large contrast in intensity, so that the dimmer, diffuse corona tends to be underexposed, which may make SXT sightings of the wave difficult.

Rust & Svestka (1979) describe slowly moving (from ~400 down to ~10 km s^{-1}) disturbances seen in images from a soft X-ray telescope on *Skylab*, which had a wavelength coverage similar to SXT's (but including somewhat longer wavelengths) of approximately 2–54 Å. Those disturbances were weak, only hinting at wave structures, in contrast to the clear features seen by EIT. This may be evidence that the EIT wavelike feature is less apparent in *Skylab*- or SXT-type instruments because of the physical properties of the wave, rather than a problem with data coverage. It will be necessary to investigate other such EIT wave events with better SXT coverage in order to resolve this question.

4. DISCUSSION

There have now been several examples of X-ray coronal dimming reported from the SXT data; it could become an important diagnostic for early-phase CME studies. Here we have seen that X-ray observations show evidence of mass loss from the low corona near the time of the launching of a halo CME event. From our mass estimates, we believe that at least a part of the CME mass was detected via the X-ray dimming.

This event appears to be a related to the "transient coronal hole" type in the classification scheme of Hudson & Webb (1997). This terminology may not be fully appropriate here, however, since by extending our difference image observations, we find that the "transient" coronal hole regions (R1 and R2) still existed 3 days after the flare's occurrence. We cannot determine if the intensities of these regions are as low as those of true coronal holes, consisting of open field lines. Furthermore, those dimming regions coincide with inner parts of dimming regions produced by an earlier, weaker flare, peaking near 0 UT on April 7. Thus it seems unlikely that these dimming regions are coronal holes according to a strict definition, since the same corona would not be expected to form two consecutive long-lived open field regions in the same location.

From our observations, it seems plausible that regions R1 and R2 could be the legs or feet of a flux rope, in the pattern described by Moore & LaBonte (1979; see also, e.g., Hirayama 1974). Prior to the flare, a portion of the flux system could be identified with the S-shaped structure in Figure 2*a*, whose shape may imply the existence of a large-scale current flow (e.g., Canfield, Pevtsov, & Acton 1995; Rust & Kumar 1996; Pevtsov, Canfield, & McClymont 1997; for a different view, see Priest & Milne 1980, who argue that sheared coronal structures may result from potential fields). Weaker dimming structures extending from the active region to the southeast and (less obviously) to the northwest would also be related to the flux rope. In this picture the stronger magnetic fields in the core of

the active region restrain the field lines at the center, but the extremities can bulge out into "elbows" (see the magnetostatic simulations of Antiochos, Dahlburg, & Klimchuk 1994). During the flare, this structure would move upward unstably and create the cusp of Figure 2*b*, because the field is forced into an opposed geometry or has been reconnected. The flux rope would propagate out as the CME into the solar wind, where it could be observed as a magnetic cloud (e.g., Burlaga 1991). Region R3 of Figure 2*d*, which is less prominent than R1 or R2, may be more tenuous coronal material, dragged along by the eruption of the flux rope, or it may be a peripheral part of it (an "elbow"). From the present SXT data, we do not have a complete view of the relationship between the dimmed coronal mass and the mass distribution in a CME as observed in white light, but a substantial fraction of the CME mass could have come from the low corona in our dimming regions.

Transient coronal holes seen with SXT have been interpreted in terms of flux ropes in several previous studies (e.g., Watari et al. 1995; Kozuka et al. 1995; Manoharan et al. 1996; Smith et al. 1997). There were no corresponding direct observations of CMEs for these previous studies, but the event reported by Smith et al. resulted in an interplanetary magnetic cloud that is consistent with our interpretation in terms of a flux rope.

Whereas the flux rope picture seems reasonable, it may be surprising that the principal dimming regions, and the photospheric intersection of the flux rope, would occur so close to the core of the active region; the center-to-center spacing of the R1 and R2 is about 120,000 km. This subtends an angle of about 10° at the center of the Sun, as opposed to an average CME angular width of 47° (Hundhausen 1993). In contrast, in the 1994 October 25 event studied by Manoharan et al. (1996), the coronal hole separation was a substantial fraction of the solar disk. It is also interesting that the dimming regions in our study persist so long (more than 3 days). Rust (1983), for example, found that for 18 transient coronal holes seen with the S-054 soft X-ray telescope flown on the *Skylab*/ATM mission (1973–1974), none lasted for more than 48 hr. Also, the transient coronal hole observed by Kozuka et al. (1995) lasted only about 17 hr. A fuller analysis of the *SOHO* and *Yohkoh* data on this event may help in understanding these issues.

The authors thank H. Gursky of NRL for suggesting and encouraging this investigation, and J. Gurman, C. St. Cyr, B. Thomson, and the *SOHO* team for providing a preview of the *SOHO* results in advance of publication. The authors also thank L. Acton, D. Alexander, and L. Culhane for fruitful discussions. National Solar Observatory/Kitt Peak data used here are produced cooperatively by NSF/NOAO, NASA/GSFC, and NOAA/SEL. A. C. S. acknowledges support from the Naval Research Laboratory/ONR basic research program. NASA supported the work of H. S. H. via contract NAGW-4578. *Yohkoh* is a mission of the Institute of Space and Astronautical Sciences (Japan), with participation from the United States and the United Kingdom.

REFERENCES

Antiochos, S. K., Dahlburg, R. B., & Klimchuk, J. A. 1994, ApJ, 420, 41
Athay, R. G., & Moreton, G. E. 1961, ApJ, 133, 935
Burlaga, L. F. 1991, in Physics of the Inner Heliosphere, Vol. 2, ed. R. Schwenn & E. Marsch (Berlin: Springer), 1
Brosius, J. W., Davila, J. M., Thomas, R. M., Saba, J. L. R., Hara, H., & Monsignori-Fossi, B. 1997, ApJ, 477, 969
Canfield, R. C., Pevtsov, A. A., & Acton, L. W. 1995, Eos, 76, S235
Delaboudinière, et al. 1995, Sol. Phys., 162, 291
Gosling, J. T. 1996, ARA&A, 34, 35
Hansen, R. T., Garcia, C. G., Hansen, S. F., & Yasukawa, E. 1974, PASP, 86, 500
Hiei, E., Hundhausen, A., & Sime, D. 1993, Geophys. Res. Lett., 20, 2785
Hirayama, T. 1974, Sol. Phys., 34, 389
Howard, R. A., Michels, D. J., Sheeley, N. R., & Koomen, M. J. 1982, ApJ, 263, L101
Hudson, H. 1996, in IAU Colloq. 153, Magnetodynamic Phenomena in the Solar Atmosphere—Prototypes of Stellar Magnetic Activity, ed. Y. Uchida, T. Kosugi, & H. S. Hudson (Dordrecht: Kluwer), 89
Hudson, H. S., Acton, L. W., & Freeland, J. R. 1996, ApJ, 470, 629
Hudson, H. S., & Webb, D. F. 1997, Geophysical Monographs 99, Coronal Mass Ejections, ed. N. Crooker, J. Joselyn, & J. Feynman (Washington: AGU), 27
Hundhausen, A. 1993, J. Geophys. Res., 98, A8, 13,177
Kahler, S. 1992, Annu. Rev. Astron. Astrophys., 30, 113
Kozuka, T., Watanabe, T., Kojima, M., Ohyama, M., Tsuneta, S., Khan, J. I., & Watari, S. 1995, PASJ, 47, 377
Low, B. C. 1997, Sol. Phys., 167, 217
Manoharan, P. K., van Driel-Gesztelyi, L., Pick, M., & Demoulin, P. 1996, ApJ, 468, L73
McAllister, A. H., Dryer, M., McIntosh, P., Singer, H., & Weiss, L. 1996, J. Geophys. Res., 101, 13, 497
Moore, R. L., & LaBonte, B. 1979, in IAU Symp. 91, Solar and Interplanetary Dynamics, ed. M. Dryer & E. Tandberg-Hanssen (Dordrecht: Reidel), 207
Pevtsov, A. A., Canfield, R. C., & McClymont, A., N. 1997, ApJ, 481, 973
Priest, E. R., & Milne, A. N. 1980, Sol. Phys., 65, 315
Rust, D. M. 1983, Space Sci. Rev., 34, 21
Rust, D. M., & Hildner, E. 1976, Sol. Phys., 48, 381
Rust, D. M., & Kumar, A. 1996, ApJ, 464, L199
Rust, D. M., & Svestka, Z. 1979, Sol. Phys., 63, 279
Shibata, K., Masuda, S., Shimojo, M., Hara, H., Yokoyama, T., Tsuneta, S., Kosugi, T., & Ogawara, Y. 1995, ApJ, 451, L83
Smith, Z., Watari, S., Dryer, M., Manoharan, P. K., & McIntosh, P. S. 1997, Sol. Phys., 171, 177
Sterling, A. C. 1997, ApJ, 478, 807
Sterling, A. C., Hudson, H. S., & Watanabe, T. 1997, ApJ, 479, L149
Tsuneta, S., et al. 1991, Sol. Phys., 136, 37
Watari, S., Kozuka, T., Ohyama, M., & Watanabe, T. 1995, J. Geomagn. Geoelectr., 47, 1063

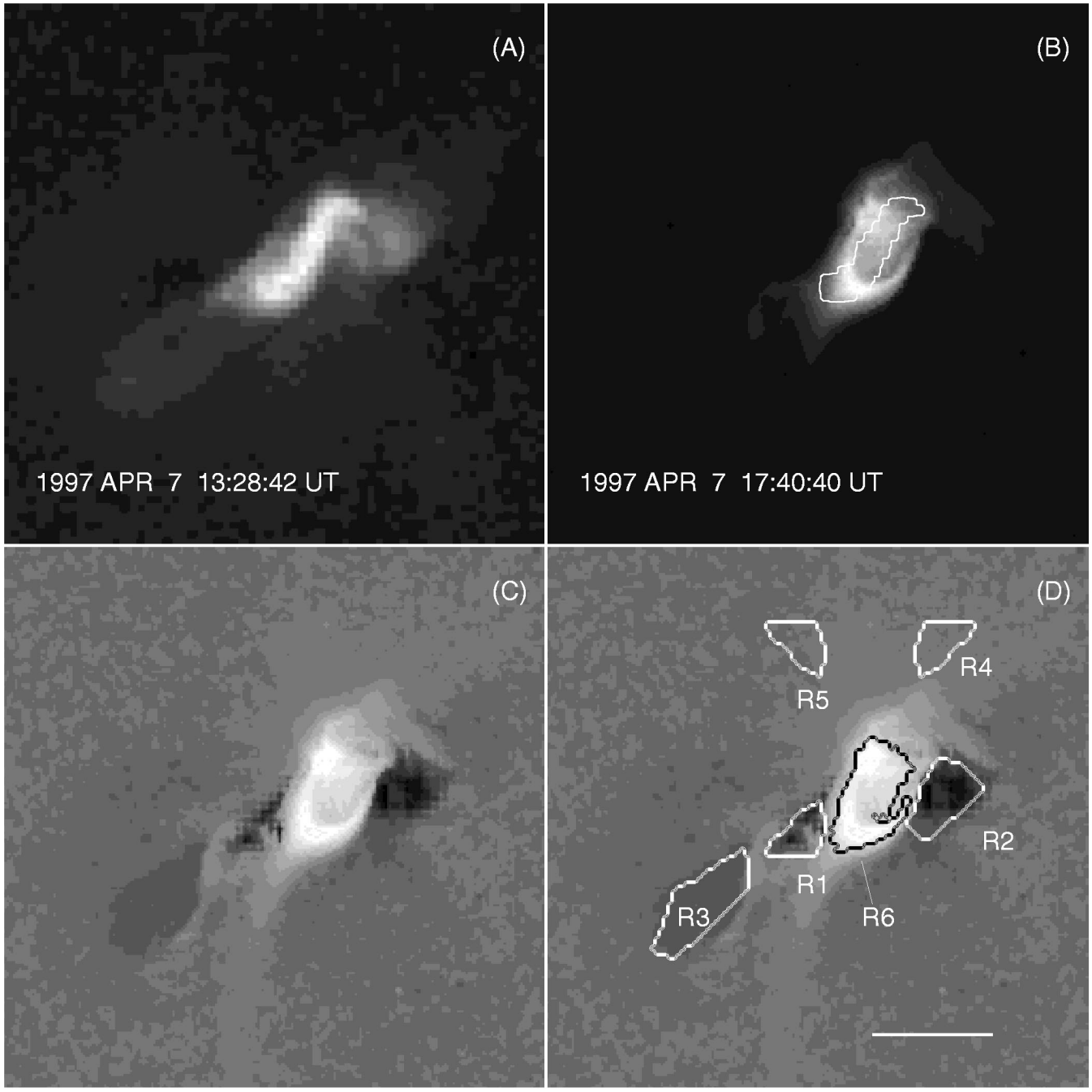

FIG. 2.—Images from the AlMg filter of SXT (*a*) prior to the CME-related flare, and (*b*) late in the decay phase of the CME flare. In these images north is up and west to the right. The contour in (*b*) is the 40% intensity contour from the image in (*a*). (*c*) Difference image formed by subtracting the image in (*a*) from that in (*b*). (*d*) As in (*c*), with R1 and R2 showing the strongest dimming regions, R3 showing a third dimming region, R4 and R5 covering regions without any dimming, and R6 denoting the brightest 75% intensity contour from the image in (*b*). The bar in (*d*) is a 100,000 km length scale. Other dimming regions also occurred, but they are not clearly visible in this figure. To represent the difference images, we have used square-root compression separately on the positive and negative areas.

STERLING & HUDSON (see 491, L56)

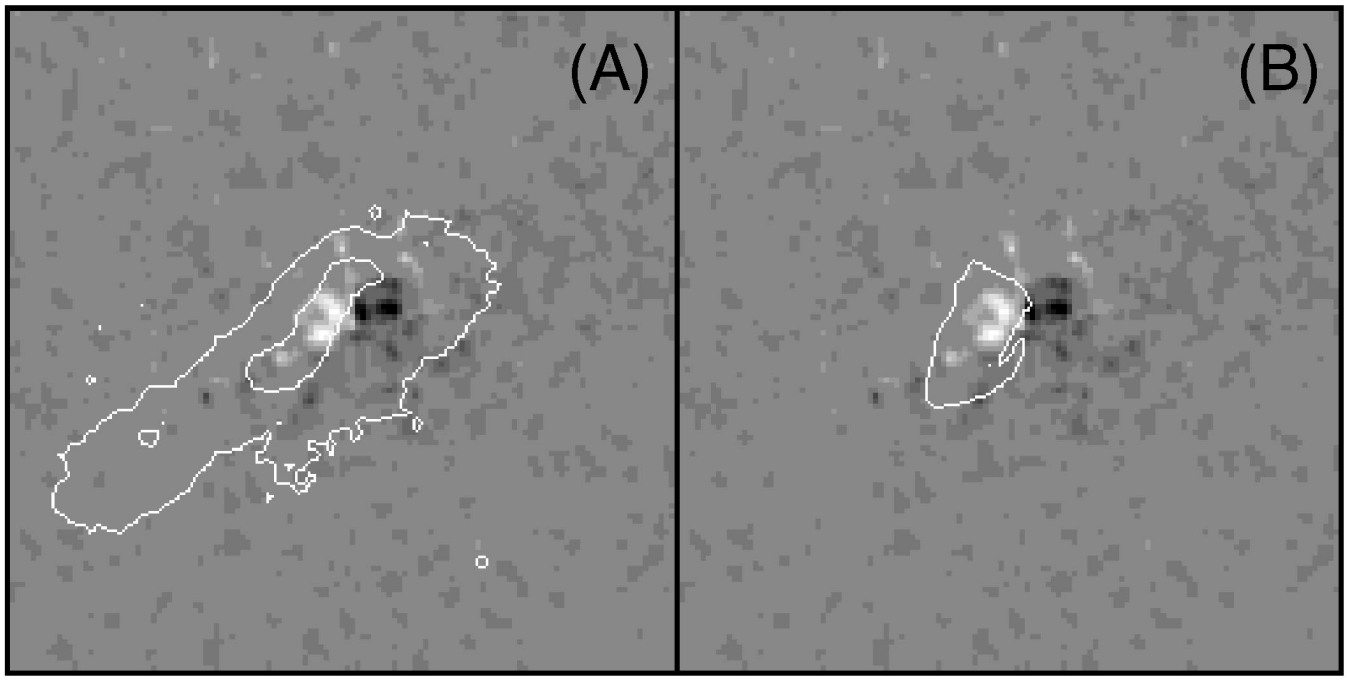

FIG. 3.—(*a*) Magnetogram from 16:14 UT on 1997 April 7, with positive polarity shown as white. Overlaid are 20% and 1% contours of the preflare image of Fig. 2*a*. (*b*) Same magnetogram as in (*a*), overlaid by 25% contours of the flare decay-phase image shown in Fig. 2*b*.

STERLING & HUDSON (see 491, L56)